



Topography optimization of an enclosure panel for low-frequency noise and vibration reduction using the equivalent radiated power approach

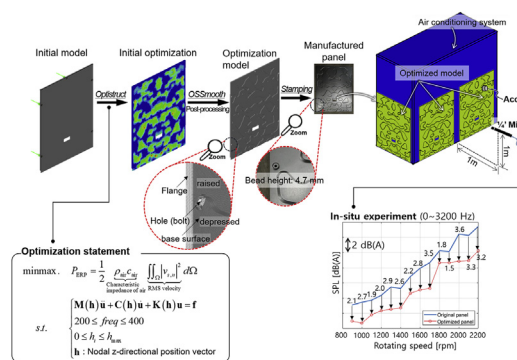
Hyun-Guk Kim¹, Can Nerse¹, Semyung Wang^{*}

School of Mechanical Engineering, Gwangju Institute of Science and Technology, 123 Cheomdangwagi-ro, Buk-gu, Gwangju 61005, Republic of Korea

HIGHLIGHTS

- Low-frequency noise is reduced by a design optimization of enclosed panel.
- Topography optimization process is implemented using Altair OptiStruct.
- The performance of noise and vibration of the enclosed panel is verified with in-situ experiment.

GRAPHICAL ABSTRACT



ARTICLE INFO

Article history:

Received 30 May 2019

Received in revised form

6 August 2019

Accepted 14 August 2019

Available online 15 August 2019

Keywords:

Topography optimization

Equivalent radiated power

Air conditioning system

Stamping

In-situ experiment

ABSTRACT

An enclosure panel is widely used in industrial applications. The panel under a dynamic loading excites the surrounding air medium and noise is radiated into the acoustic space. The radiated sound can be suppressed by having changes in the structure. The noise reduction performance can be further improved by a design optimization. In this study, a topography optimization is conducted to design an enclosure panel. Topography optimization results in a bead pattern, which helps maintain the thickness at a constant level throughout the structure. The final optimized structure can be manufactured using a stamping process. Compared with other optimization methods, topography optimization requires minimal manufacturing effort and cost, with no additional increase in mass. Moreover, this type of optimization is effective for noise reduction problems because no holes are created in the structure. In this study, the objective function selected to minimize the low-frequency noise is the equivalent radiated power. The topography optimization of the enclosure panel has been conducted using the commercial software Altair OptiStruct, with loads and constraints considered. In order to verify the optimization result, in-situ experiment was performed with panels produced by the stamping process.

© 2019 The Authors. Published by Elsevier Ltd. This is an open access article under the CC BY-NC-ND license (<http://creativecommons.org/licenses/by-nc-nd/4.0/>).

1. Introduction

Recently, air conditioners have been more commonly installed as built-in systems in the construction process of a building. In conventional air conditioning systems, an outdoor unit operates with a paired indoor unit. However, with the rapid increase in the

* Corresponding author.

E-mail address: smwang@gist.ac.kr (S. Wang).

¹ These authors have equally contributed in this work.

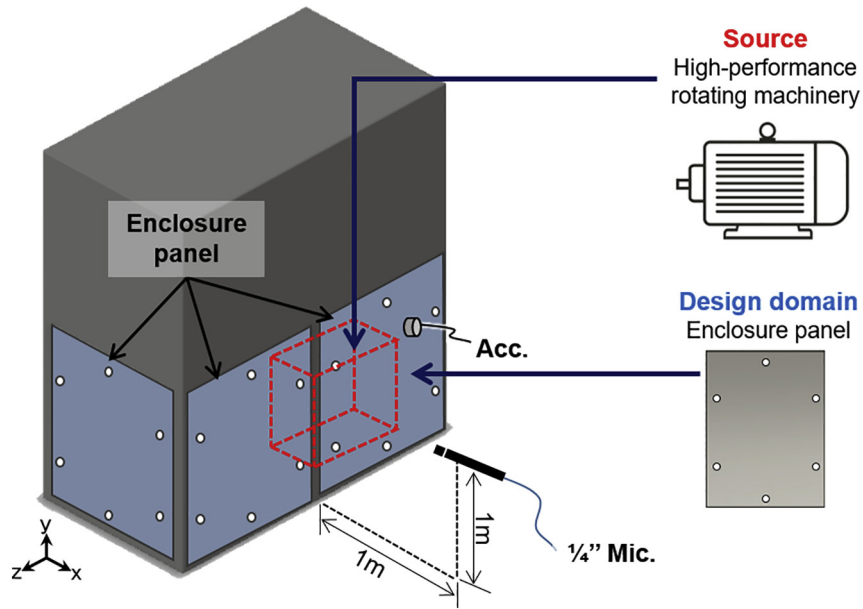


Fig. 1. Experimental setup of the air conditioning system excited by the rotating machinery.

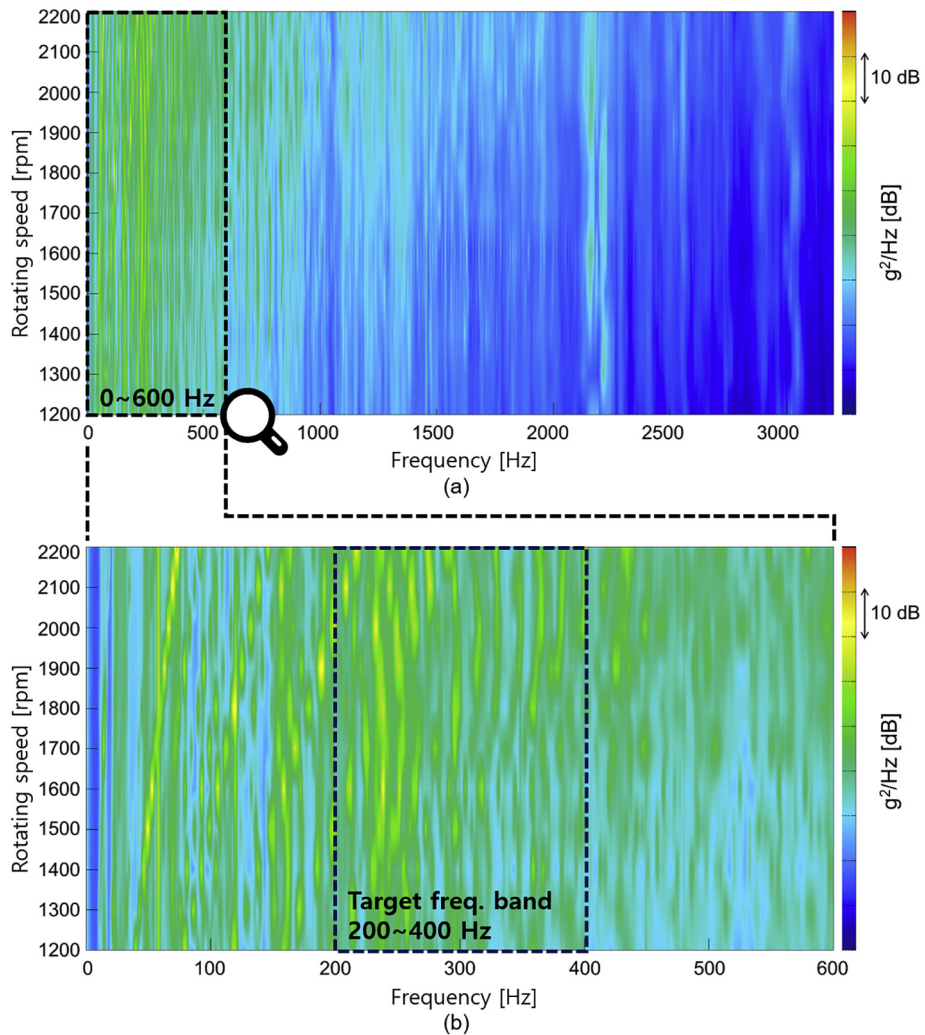


Fig. 2. Power spectral density (PSD) of the reference accelerometer in the frequency range of (a) 0–3200 Hz, and (b) 0–600 Hz.

number of indoor units in a building, central air conditioning systems have been developed to cover several indoor units. The conventional central air conditioning systems are powered by an electric heat pump that converts electrical energy to mechanical energy along the axial direction. To enhance the performance of the outdoor unit in the central air conditioning system, high performance rotating machinery has been used in the system. The air conditioning systems with high performance rotating machinery have high power output and efficiency. However, the drawback is that the noise is vastly increased due to the operation of the rotating machinery.

Among the many types of noise propagation, a structure-borne noise, which is induced by rotational machinery, is transmitted through solid structures and radiated into acoustic space, similar to the case of an automobile [1]. In a typical outdoor unit of an air conditioning system, the sound emanates from the enclosure panels, which are installed on all sides.

In industrial applications, noise and vibration problems have been commonly solved by implementing passive sound and vibration control. To improve the noise insulation performance based on passive control, damping materials have been widely used [2,3]. In 2007, Li and Liang studied the sound power reduction by attaching a damping layer on a steel panel subjected to a unit harmonic force [2]. The thicknesses of the damping layer and base panel were determined using the response surface method to minimize the sound power of the damped structure. In 2016, Qin et al. conducted a study to minimize the sound pressure level at the center node in an enclosure [3]. The damping layer attached on top of the enclosure was divided into several parts, and the thickness of each part was optimized using the response surface method. However, while most damping material-based noise reduction approaches provide good insulation at high frequencies, the sound absorption performance at low frequencies (<500 Hz) is poor [4]. In practice, reinforcements have also been used for vibration control as in the case of fuselage sections of aircrafts [5,6].

Design optimization has been implemented to improve structural behavior with regard to compliance and natural frequency. Among the well-known design optimization methods, topology optimization, which involves optimizing the material layout for a given set of loads and constraints, is widely used for solving vibration problems. However, in topology optimization, the volume constraint results in regions with void materials. Therefore, it is inappropriate for problems where sound radiation is a concern, because the noise escapes through the hole [7]. Topometry/reinforcement optimization is a specific case of sizing optimization, wherein the optimal thickness distribution on each element is found individually. It has been used to find the thickness distribution required to reinforce the gear box of a car to reduce the structure-borne sound [8]. However, this design approach has a disadvantage in that the mass is increased, requiring more labor to manufacture and assemble the system.

Unlike the topometry optimization, wherein the mass increases with respect to thickness variation, topography optimization, which is a specific type of shape optimization, generates a stiffer structure while yielding a minimal mass increase, because this optimization maintains a constant thickness throughout the structure [7]. In topography optimization, a perturbation vector is applied to each node in the design domain along the normal direction, resulting in a bead pattern in the optimized structure [9]. Recently, topography optimizations have been performed on structural designs in practical applications. In 2006, topography optimization was used to maximize the natural frequency of the first bending mode for the heat shield on a vehicle [10]. This study was performed using the commercial software GENESIS. In 2011, topography optimization was used to reduce the transient vibration response of an engine block of a vehicle [11]. In 2012, topography

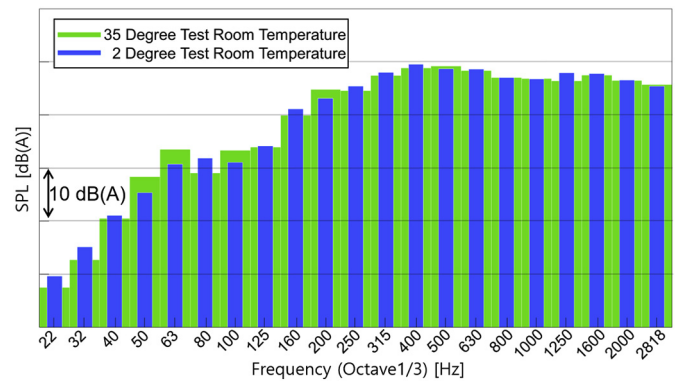


Fig. 3. 1/3 octave band comparison with respect to the test room temperature at a rotating speed of 2200 rpm.

optimization under transient loading was comparatively studied based on various design sensitivity analysis methods [12]. In 2013, a research was conducted to optimize the equivalent radiated power of an automobile oil pan [13]. The sound power was reduced by 20% compared with its initial state. In another study, topography optimization was applied to a wishbone suspension of an automobile using OptiStruct and Abaqus. The residual stress was reduced, whereas the natural frequency was increased [14]. In 2016, a topography optimization of a gear box of an automatic transmission was conducted to reduce the vibration response [15]. This optimization technique has been largely used in the solution of NVH (noise, vibration, and harshness) problems. The bead pattern generated by topography optimization of a flat surface can be fabricated by stamping or deep drawing processes [15,16]. To reduce the manufacturing cost and improve the noise insulation performance, designing the enclosure panel by topography optimization is considered as an ideal solution. In this study, the topography optimization of an enclosure panel is conducted to minimize the noise generated by an air conditioning system.

The rest of this paper is organized as follows. In Section 2, the topography optimization and a finite element model of the enclosure panel with loads and constraints are described. The objective function selected to minimize the noise radiated from the panel is formulated using the equivalent radiated power. The optimization process using Altair OptiStruct is described in detail. Section 3 discusses the performance of the optimized panel fabricated using the stamping process, in comparison with that of the original panel. Finally, Section 4 presents the conclusions of this study.

2. Topography optimization of an enclosure panel

The central air conditioning system has two main operating cycles based on climate conditions. One operating cycle is associated with the winter weather condition in which the system

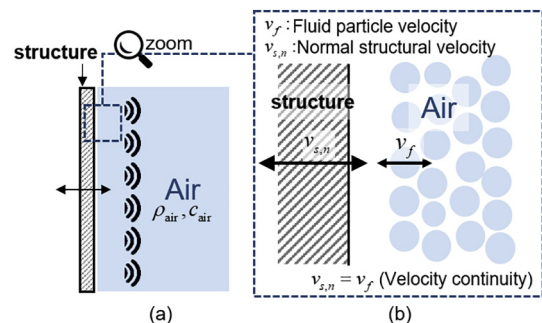


Fig. 4. (a) Schematic of the vibro-acoustic interaction in the boundary between the structure and the air medium, (b) the details of the interaction in (a).

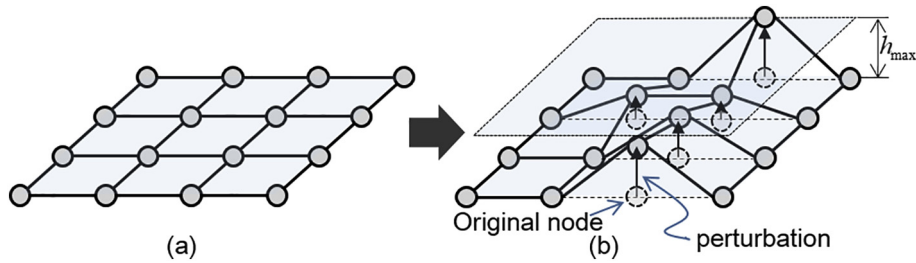


Fig. 5. Concept of topography optimization: (a) initial model, (b) optimization model where h_{max} is the maximum bead height.

operates to warm the desired space. The other operating cycle is run for the summer weather condition in which cooling occurs. The high-performance rotating machinery is the main power source for both climate conditions. In a typical air conditioning system, the operating speed of the rotating machinery varies with respect to climate mode. In the current application it was set to change between 900 and 2200 rpm (rpm). In order to identify the system parameters a set of experiments were conducted. Fig. 1 shows the experimental setup of the air conditioning system. The location of the excitation source with respect to panels, and transducers are shown.

In the preliminary operational measurements, the power spectral density (PSD) with respect to the rotating speed revealed that the response of the source is dominant at approximately 3 kHz for all rotating speeds [17,18]. However, the magnitude of the response of the enclosure panel is noticeable in the low-frequency range (<1 kHz). Regardless of the weather condition or the rotating speed, the acceleration response of the enclosure panel appears to be relatively higher in the frequency range of 200–400 Hz, as shown in Fig. 2. Observing the noise level in the A-weighted 1/3 octave band plot in Fig. 3, it is deduced that the frequency bands that contribute most to the audible noise are in the range of 0–600 Hz. The identified frequency band of 200–400 Hz has been considered the target frequency band for this application.

2.1. Equivalent radiated power (ERP)

In systems with enclosure panels, vibrating panel structure excites the surrounding air medium and radiates noise. Fig. 4 shows a

schematic of this vibro-acoustic interaction.

The sound power in the air medium is expressed as follows.

$$P = \iint_{\Gamma} I \cdot \vec{n} \, d\Gamma \text{ where } I = \frac{1}{2} \text{Re}(p\mathbf{v}), \tag{1}$$

where I , \vec{n} , Γ , p , and \mathbf{v} are the acoustic intensity, normal vector, structure-air interface, radiated acoustic pressure, and particle velocity vector of air, respectively [19–21]. The acoustic intensity is defined as the power carried by the acoustic wave per unit area in the direction normal to the surface. The sound power for the radiated noise is expressed as the surface integral of the acoustic intensity along the normal direction at all points on a given surface Γ . In the vibro-acoustic problem, the structural velocity is equal to the air particle velocity at the boundary between the surface and the air medium. This is called the velocity continuity, which is expressed as follows.

$$v_{s,n} = v_{\text{air}} = \frac{p}{\rho_{\text{air}} c_{\text{air}}}, \tag{2}$$

where $v_{s,n}$, v_{air} , ρ_{air} , c_{air} , and p are the structural normal velocity, particle velocity of air, air density, speed of sound in air, and acoustic pressure, respectively. By substituting Eq. (2) into Eq. (1), the equivalent sound power emitted from the vibrating structure can be expressed as a function of the vibration velocity of the structure. The equivalent radiated power used in this study is expressed as follows.

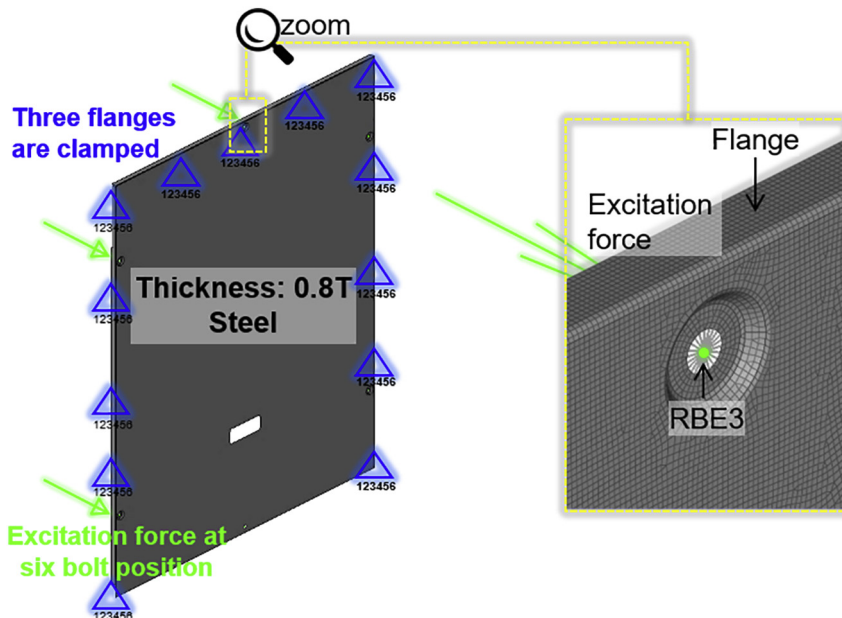


Fig. 6. Finite element model of an enclosure panel to compute the equivalent radiated power.

Table 1
Bead parameters for the topography optimization.

| Parameter | Value |
|---------------------|-------|
| Minimum width | 10 mm |
| Maximum bead height | 5 mm |
| Bead angle | 45° |

$$P_{ERP} = \frac{1}{2} \rho_{air} c_{air} \iint_{\Gamma} |v_{s,n}|^2 d\Gamma = \frac{1}{2} \rho_{air} c_{air} \sum_{e=1}^{N_e} A_e |v_{s,n}|^2, \quad (3)$$

where A_e and N_e are the elementary surface area and element number in domain Γ , respectively. In a finite element analysis (FEA), the integral equation can be expressed in terms of a summation as shown in the second term of Eq. (3). The level of the equivalent radiated power (L_{ERP}) can be expressed as follows.

$$L_{ERP} = 10 \log \left(\frac{P_{ERP}}{P_{ref}} \right) \text{ [dB]} \quad \text{where } P_{ref} = 10^{-12} \text{ [W]} \quad (4)$$

2.2. Optimization setup

Topography optimization is a specific case of shape optimization [7]. In shape optimization, each node can be perturbed in all directions, whereas in topography optimization the nodes can be perturbed only in the z-direction from its initial position. In a topography optimization process, which is shown in the conceptual diagram in Fig. 5, the structure surface is modified iteratively until the objective function is satisfied. Hence, the optimized structure features a bead pattern.

In this study, the design domain is the enclosure panel of the air conditioning system outdoor unit. The system is enclosed by six panels. Each panel is fixed on the supporting frame by six bolts. The edges are considerably rigid because of the flanges on left, right,

and top positions. The panels are identical, that is, they have the same material property, assembly condition, size, and shape. The nodes located at each bolt hole are interconnected by rigid body elements (RBE3) [22]. The excitation forces act on independent nodes located at the center of each RBE3 element. As the three edges (top, left, and right) on the panel are enclosed by a relatively rigid supporting frame, a clamped boundary condition is considered on the three edges, as shown in Fig. 6.

To reduce the analysis time, the enclosure panel was changed to a shell structure with a constant thickness using the mid-surface because the width and length of the panel are considerably greater than its thickness. The optimization statement is expressed as follows.

$$\begin{aligned} \text{minmax.} \quad & P_{ERP} = \frac{1}{2} \rho_{air} c_{air} \iint_{\Omega} |v_{s,n}|^2 d\Omega, \\ & \text{Characteristic RMS velocity} \\ & \text{impedance of air} \\ \text{s.t.} \quad & \begin{cases} \mathbf{M}(\mathbf{h})\ddot{\mathbf{u}} + \mathbf{C}(\mathbf{h})\dot{\mathbf{u}} + \mathbf{K}(\mathbf{h})\mathbf{u} = \mathbf{f}, \\ \text{where } \mathbf{u} = \tilde{\mathbf{u}}e^{j\omega t}, \mathbf{f} = \tilde{\mathbf{f}}e^{j\omega t}, \\ f_{min} (= 200\text{Hz}) \leq \text{freq} \leq f_{max} (= 400\text{Hz}), \\ 0 \leq h_i \leq h_{max} (= 2\text{mm}), \\ \mathbf{h} : \text{design variable vector,} \end{cases} \end{aligned} \quad (5)$$

where \mathbf{M} , \mathbf{C} , \mathbf{K} , \mathbf{F} , \mathbf{u} , h_{max} , and \mathbf{h} are the global mass, damping, stiffness matrices, force vector, displacement vector, maximum bead height, and vector of design variables h_i , respectively. As mentioned above, the target frequency band ranges from f_{min} (200 Hz) to f_{max} (400 Hz). In this study, the design optimization is conducted as a minmax problem, which involves minimizing the maximum equivalent radiated power P_{ERP} within a target frequency band at each iteration.

To build the topography optimization model to minimize the equivalent radiated power, several parameters were needed to be defined. In this study, the speed of sound propagation, material

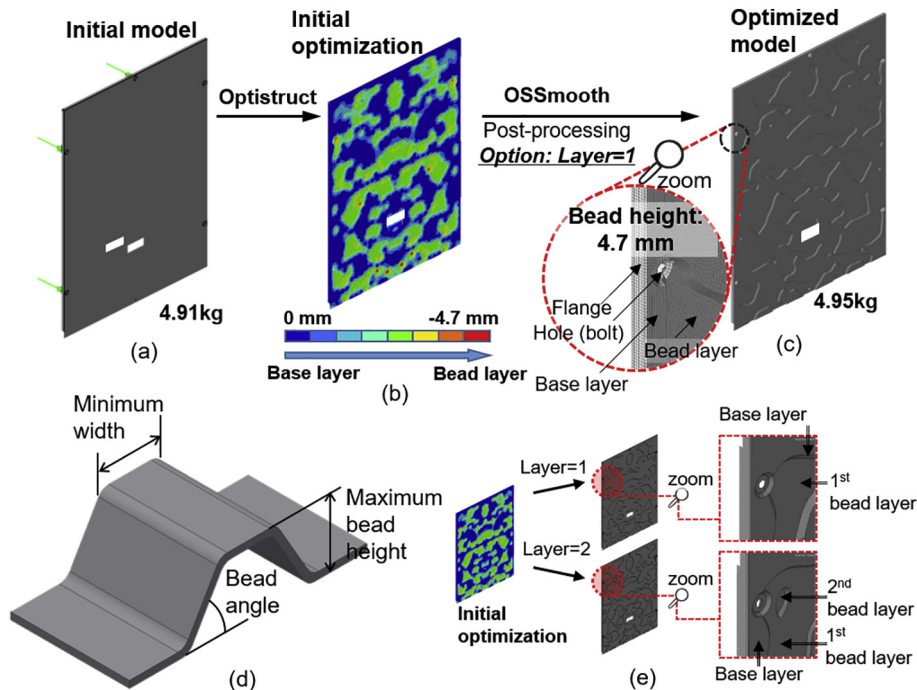


Fig. 7. Optimization result: (a) initial model, (b) initial optimization using OptiStruct, (c) optimized model using OSSmooth, (d) user-defined parameter description for topography optimization, and (e) layer options in OSSmooth.

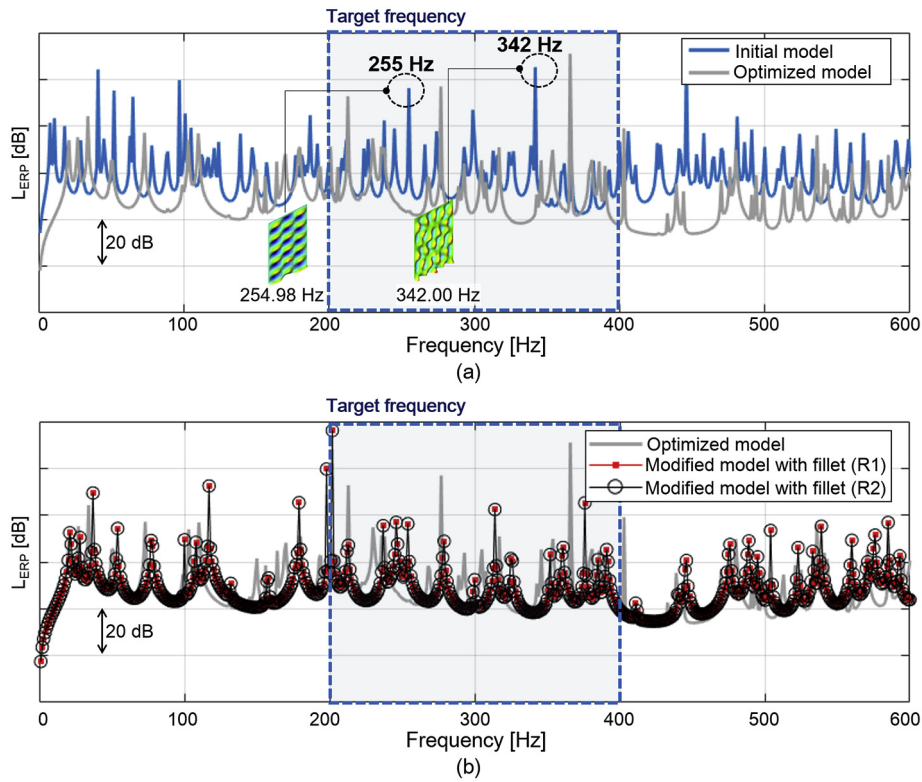


Fig. 8. Equivalent radiated power of (a) initial model and optimized model using Altair OptiStruct and OSSmooth in Fig. 5, and (b) optimized model and modified model with rounded fillet (R1, R2).

density of air, and reference sound power were set as 343 m/s, 1.2 kg/m^3 , and 10^{-12} W , respectively. The sequential quadratic programming (SQP) algorithm was used as the optimization algorithm. The SQP algorithm is one of the most successful methods for

a large scale constrained optimization problem [23,24]. The minimum width, maximum bead height, and bead angle are the constraints in the optimization problem. They determine the bead shape of the optimized structure. Table 1 lists these parameters.

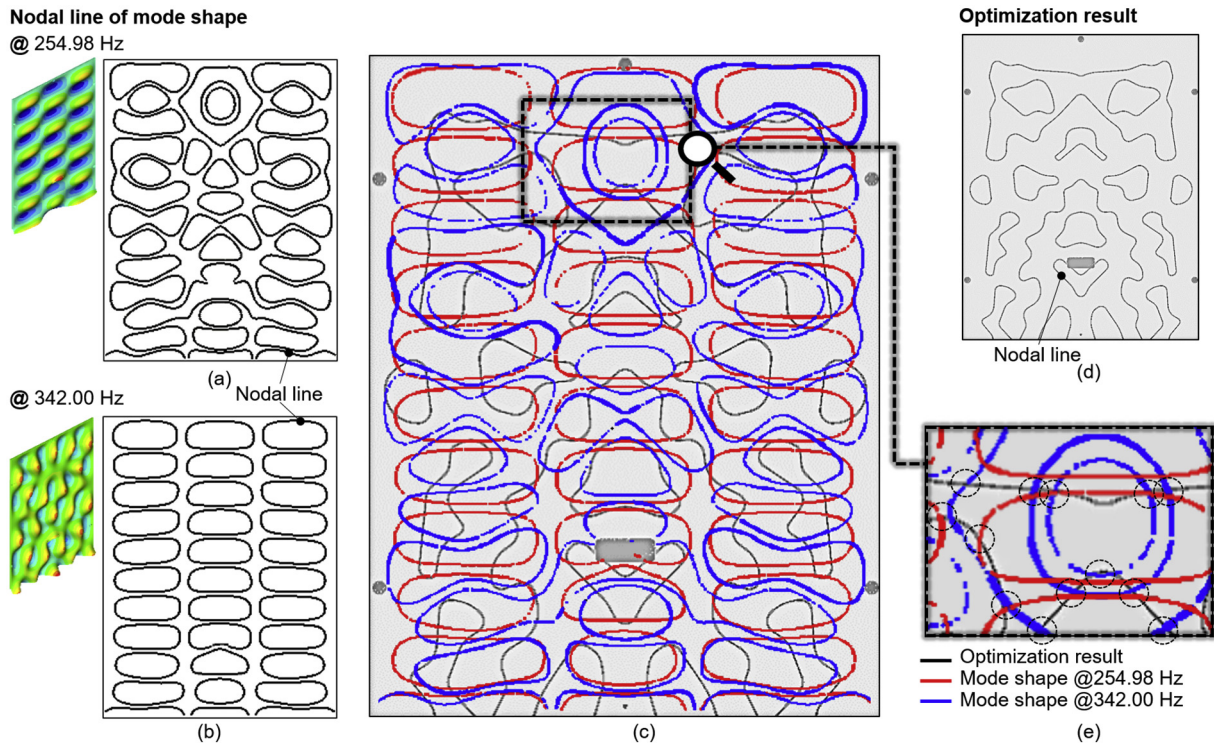


Fig. 9. Physical interpretation of the optimization result; nodal lines of mode shapes of the initial model at (a) 254.98, (b) 342.00 Hz and (d) optimal bead design; (c) a comparative view of the nodal lines; (e) zoom view of Fig. 9(c).

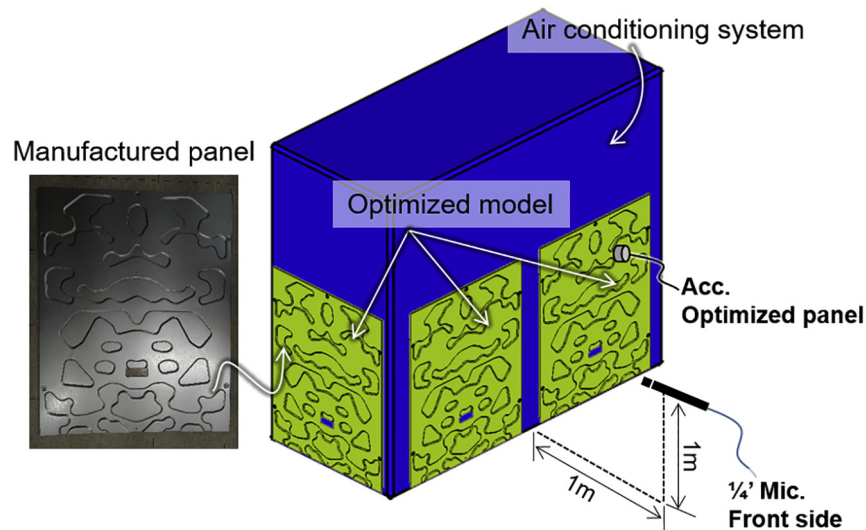


Fig. 10. In-situ experimental setup for verification of the optimized panel.

2.3. Optimization results

This section presents the results of the topography optimization defined in Section 2.2. To solve the optimization problem, the Altair OptiStruct was used [13,14]. Fig. 7 shows the optimization results.

Fig. 7(a) shows the initial model of the panel. Fig. 7(b) shows the initial optimization result, which was obtained by the OptiStruct solver [22]. However, this structure cannot be manufactured directly because of its complex shape. Therefore, the OSSmooth, which is a post-processor in OptiStruct, is applied to the optimized model, as shown in Fig. 7(c). The color of the initial optimization represents the height of the bead. The nodes on the base panel where no deformation occurs are indicated in blue. Fig. 7(d) shows the parameters for the topography optimization, which was listed in Table 1. The resultant shape of the topography optimization is determined by these user-defined parameters. Fig. 7(e) shows the concept of the layer options in OSSmooth. In the case where layer equals one, two layers are generated, namely a base layer and a bead layer, whereas three layers (a base layer and two bead layers) are generated in the case where layer equals two. With the increase in the number of layers, the manufacturing cost of the panel increases significantly because of the increase in complexity of the bead shape. As it is shown in Section 3, an optimized model corresponding to layer = 1 was employed for experimental verification. Fig. 8 shows the calculated equivalent radiated power (L_{ERP}) for each case.

As shown in Fig. 8(a), the equivalent radiated power of the optimized model is reduced by 5.9 dB at a target frequency band of 200–400 Hz compared with the initial model, whereas in the frequency band of 0–600 Hz, it is reduced by approximately 9.4 dB. However, in the manufacturing process using stamping, the fillet must be applied to the bead pattern of the optimized model because of the limitations in producing hard-edged corners. Two modified models were created by applying fillets with dimensions of 1 and 2 mm, corresponding to R1 and R2 in Fig. 8(b). Fig. 8(b) shows the equivalent radiated power of the modified models. In the frequency range of 0–600 Hz, the equivalent radiated power of the modified model with R2 fillet is reduced by 8.59 dB, compared with the initial model. However, as shown in Fig. 7, the mass increase in the optimization process is only 0.6%. Thus, topography optimization significantly improves noise insulation with minimal increase in the mass.

As shown in Fig. 8a, the initial model has a high equivalent radiated power at 255 and 342 Hz within the target frequency band

(200–400 Hz). These frequencies correspond to the vibrating modes (254.98 and 342.00 Hz). Fig. 9(a), (b) show the nodal lines of the vibrating modes of the initial model at 254.98 and 342.00 Hz, respectively. Fig. 9(d) is the contour of the optimization result. Fig. 9(c) is a comparative view that overlaps these two nodal lines and the contour. Fig. 9(e) is the zoom view of Fig. 9(c). In Fig. 9(c), the black (–), red (–), and blue (–) lines represent the nodal lines for the mode shapes at 254.98, 342.00 Hz and the bead shape of the optimization result, respectively. The nodal line of the bead shape shows a tendency to cross the nodal lines of the two mode shapes. This results in a stiffer structure that reduces the bending deformation and minimizes the velocity response corresponding to these mode frequencies. Thus, the objective function, which is the equivalent radiated power of the panel, is satisfied as shown in Eq. (5). Section 3 demonstrates the noise and vibration evaluation of the manufactured panel that is based on the modified model with R2 fillet (Fig. 8b).

3. Experimental verification

To verify the performance of the air-conditioning system covered with the optimized panels, a set of experiments were conducted. Two main weather conditions were tested for this specific unit, as mentioned in Section 2. For the summer condition, the temperature inside the test room was set at a constant temperature of 35 °C, and to simulate the winter weather, the test room temperature was set to 2 °C. Although the experimental verification was carried out for both climate conditions, only the result with respect to winter weather condition is presented.

Fig. 10 shows the experimental setup including the locations of the transducers. A reference accelerometer was attached to the panel next to the power source to measure the acceleration response. The location of the reference accelerometer was chosen such that the vibration amplitudes of the original and optimized panels are similar [18]. To measure the acoustic pressure at a

Table 2
Operating conditions for experimental verification.

| Operating condition | Value |
|-------------------------|----------------------------------|
| Sample frequency | 6400 Hz |
| Number of lines | 3201 |
| Frequency resolution | 1 Hz |
| Time duration | 40 s |
| Operational speed cases | 900 rpm, 1000 rpm, ..., 2200 rpm |

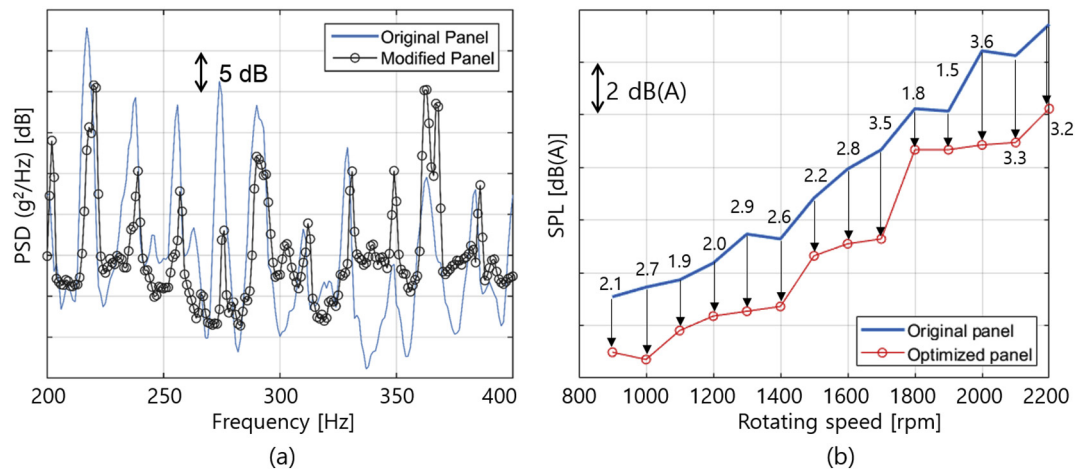


Fig. 11. Comparison of responses for original and optimized panels under operating condition: (a) PSD comparison of the reference accelerometer at the rotating speed of 2200 rpm, (b) overall A-weighted sound pressure level (0–3200 Hz) comparison of the reference microphone with respect to the rotating speed.

reference location, a GRAS $\frac{1}{4}$ " free-field microphone was placed 1 m from the panel where the accelerometer was attached, at a height of 1 m from the ground level. Table 2 lists the test parameters for the experimental verification.

Fig. 11 shows the results obtained from the operational measurements. The PSD of the reference accelerometer was compared for the original and optimized panels. At the maximum operating speed of 2200 rpm, the average reduction in the PSD magnitude was 3 dB for the entire frequency range of the test. At the target frequency range of 200–400 Hz, an average reduction of 3.1 dB was obtained, whereas in the range of 0–600 Hz, the reduction in magnitude was 3.8 dB. The results from the measured sound pressure on the reference microphone also showed a reduction for the optimized panel across all operational speed cases. A-weighted sound pressure level (SPL) that was measured at the microphone location shows a favorable result for all rotating speeds as shown in Fig. 11b. At 2200 rpm, the magnitude of reduction was measured to be 3.2 dB(A), while the average decrease was 2.6 dB(A) with respect to the original panel. Even under extreme operating conditions (≥ 2000 rpm) the optimized panel was demonstrated to perform better.

The results obtained from the modal testing and operational measurements were found to be in overall agreement with the FE simulation results shown in Section 2. In the target frequency band, the vibration response of the panel and the radiated noise decreased for the optimized system. For the frame structure connected to the enclosure panel via bolts, the assumption of clamped boundary conditions was proved accurate based on the relative rigidity of the frame. Therefore, the vibration transmission path was reduced to bolted joints for the panel. Airborne noise inside the cavity could be another excitation source; however, for the frequency range of interest, the effect of airborne noise was assumed to be insignificant. A transfer path analysis should be performed on the system to precisely determine the noise contribution; however, it was considered unnecessary given the scope of this study.

4. Conclusions

In this work, a topography optimization-based design approach was applied to an enclosure panel of an air conditioning system operated by a high-performance rotating machinery. The equivalent radiated power was employed as the objective function in the optimization procedure to quantify and minimize the noise radiated from the surface of the panel.

The optimized structure was produced through a stamping process, wherein a bead pattern is formed. The FEA results were

validated by conducting experiments on the original and manufactured optimized panels. As outlined in the paper, this type of solution to a common NVH problem can be advantageous in practical implementation when other solution techniques are considered. The following are the main advantages:

1. Compared to material-based noise insulation, such as constrained layer damping treatment or stiffeners, the mass increase resulting from the topography optimization is relatively insignificant ($<1\%$). As a result, the manufacturing cost can be reduced by applying a topography optimization-based solution procedure.
2. The structure-borne noise can be effectively reduced for a specific frequency band at low frequencies.
3. The ERP function, which adopts velocity continuity at the structure-acoustic boundary in the numerical analysis, is considered to present an upper bound on the expected reduction in the radiated noise. Although the experimental results were found to be more conservative, the ERP function can be useful to approximate the sound radiating to free acoustic space. Under controlled experimental conditions, this approximation was found to be applicable from the resulting behavior of the optimized structure.

These considerations make the solution procedure appealing for other NVH applications. The manufacturing process used in this research can be unreasonable if the source of excitation or make up of the system is changed significantly, making the optimized structure obsolete for the intended purposes. Therefore, the procedure outlined in this research is not recommended for the mid stages of product design; rather, it should be implemented on the final product.

The flexibility of damping treatments commonly utilized in practical applications can make the combined effect with topography optimization a suitable approach to further reduce the noise within the framework developed in this research. This will be explored in future studies.

CRediT authorship contribution statement

Hyun-Guk Kim: Methodology, Software, Visualization, Writing - original draft, Writing - review & editing. **Can Nerse:** Data curation, Validation, Writing - original draft, Writing - review & editing. **Semyung Wang:** Conceptualization, Supervision, Funding acquisition, Writing - review & editing.

Acknowledgements

This work was supported by a National Research Foundation of Korea (NRF) grant funded by the Korean government (NRF-2017R1A2A1A05001326).

Data statement

All data in this paper are available, there is no additional data.

References

- [1] J. Pang, *Noise and Vibration Control in Automotive Bodies*, Wiley, 2018.
- [2] Z. Li, X. Liang, Vibro-acoustic analysis and optimization of damping structure with Response Surface Method, *Mater. Des.* 28 (7) (2007) 1999–2007.
- [3] X. Qin, Y. Wang, C. Lu, S. Huang, H. Zheng, C. Shen, Structural acoustics analysis and optimization of an enclosed box-damped structure based on response surface methodology, *Mater. Des.* 103 (2016) 236–243.
- [4] C. Fuller, R. Harne, Advanced passive treatment of low frequency sound and vibration, in: *Proceedings of Acoustics2009*, 2009.
- [5] R. Vaicaitis, M. Slazak, Noise transmission through stiffened panels, *J. Sound Vib.* 70 (3) (1980) 413–426.
- [6] M. van Tooren, L. Krakkers, Multi-disciplinary design of aircraft fuselage structures, in: *45th AIAA Aerospace Sciences Meeting and Exhibit*, 2007.
- [7] T. Ide, M. Otomori, J.P. Leiva, B.C. Watson, Structural optimization methods and techniques to design light and efficient automatic transmission of vehicles with low radiated noise, *Struct. Multidiscip. Optim.* 50 (6) (2014) 1137–1150.
- [8] J. Bös, Numerical optimization of the thickness distribution of three-dimensional structures with respect to their structural acoustic properties, *Struct. Multidiscip. Optim.* 32 (1) (2006) 12–30.
- [9] J.P. Leiva, Methods for generating perturbation vectors for topography optimization of structures, in: *5th World Congress of Structural and Multidisciplinary Optimization*, 2003.
- [10] G.N. Vanderplaats, Structural optimization for statics, dynamics and beyond, *J. Braz. Soc. Mech. Sci. Eng.* 28 (3) (2006) 316–322.
- [11] X.F. Du, Z.J. Li, F.R. Bi, J.H. Zhang, X. Wang, K. Shao, Structural topography optimization of engine block to minimize vibration based on sensitivity analysis, *Adv. Mater. Res.* (2011) 318–326.
- [12] J.C. Medina, A. Tovar, Topography Optimization of Shell Structures Under Transient Loading: A Comparative Approach, *ASME 2012 International Design Engineering Technical Conferences and Computers and Information in Engineering Conference*, American Society of Mechanical Engineers, 2012.
- [13] E. Porto, Acoustic optimization of an engine oil pan concerning the equivalent radiated sound power function, in: *6th European Altair Technical Conference*, 2013.
- [14] S. Darge, S. Shilwant, S. Patil, Finite element analysis and topography optimization of lower arm of double wishbone suspension using abacus and optistruct, *Int. J. Eng. Res. Appl.* 4 (7) (2014).
- [15] T. Ide, H. Kitajima, M. Otomori, J.P. Leiva, B.C. Watson, Structural optimization methods of nonlinear static analysis with contact and its application to design lightweight gear box of automatic transmission of vehicles, *Struct. Multidiscip. Optim.* 53 (6) (2016) 1383–1394.
- [16] R. Dienemann, A. Schumacher, S. Fiebig, Topology optimization for finding shell structures manufactured by deep drawing, *Struct. Multidiscip. Optim.* 56 (2) (2017) 473–485.
- [17] Q. Zhang, S. To, Q. Zhao, B. Guo, Surface damage mechanism of WC/Co and RB-SiC/Si composites under high spindle speed grinding (HSSG), *Mater. Des.* 92 (2016) 378–386.
- [18] S. Wang, C. Nerse, H.W. Kim, Vibro-acoustic noise analysis of a washing machine, *Sens. Instrumen.* (2017) 47–53.
- [19] M. Klaerner, M. Wuehrl, L. Kroll, S. Marburg, FEA-based methods for optimizing structure-borne sound radiation, *Mech. Syst. Signal Process.* 89 (2017) 37–47.
- [20] A. Bhuwal, S. Kapdi, M. Jinto, Structural optimization techniques to design light weight and low radiated noise components, *SAE International Journal of Vehicle Dynamics, Stability, and NVH* 2 (2018) 203–212, 10-02-03-0013.
- [21] M. Kaltenbacher, *Computational Acoustics*, Springer, 2018.
- [22] Altair, *Optistruct User's Manual*, 2017.
- [23] P.T. Boggs, J.W. Tolle, Sequential quadratic programming for large-scale nonlinear optimization, *J. Comput. Appl. Math.* 124 (1–2) (2000) 123–137.
- [24] A.A. Keller, *Mathematical optimization terminology: A comprehensive glossary of terms*, Academic Press 2017.